

Hot corrosion effect of the vacuum arc melted (α_2/γ)Ti-48Al-2Nb-0.7Cr-0.3Si alloy under an environment of NaCl-Na₂SO₄ salt

Steven Magogodi^{1,2*}, Maria Mathabathe¹, Amogelang Bolokang^{1,3,4}, and Charles Siyasiya²

¹Council of Scientific Industrial Research, Materials Science and Manufacturing, Light metals, Meiring Naude Road, P O Box 395 Pretoria, South Africa.

²Department of Material Science and Metallurgical Engineering, Faculty of Engineering, Built Environment and Information Technology, University of Pretoria, South Africa.

³Department of Physics, University of the Western Cape, Private Bag X 17, Bellville 7535, South Africa

⁴Department of Physics, University of the Free State, P.O. Box 339, Bloemfontein, ZA9300, South Africa

Abstract. The Ti-48Al-2Nb-0.7Cr-0.3Si alloy comprising of α_2 -Ti₃Al and γ -TiAl phases was successfully fabricated using vacuum arc melting. To study its hot corrosion behaviour, the alloy was subjected to cyclic thermal loading under a Na₂SO₄ + 25 wt.%NaCl molten salt mixture at 900 °C for up to 60 h. Mass change per unit surface was measured to determine the corrosion kinetics of the alloy. The alloy experienced severe hot corrosion attacks up to -50.94 mg/cm². SEM indicated the formation of a mixture of TiO₂/Al₂O₃ scales on the alloy's surface. XRD confirmed the presence of hot corrosion products such as Na₂Ti₃O₇, TiO₂, Al₂O₃, and Cr₂O₃. The presence of chlorine gas in the hot corrosion environment resulted in the delamination of the protective scale on the surface, indicating its detrimental effect.

1 Introduction

High-temperature aero-engine components such as turbine blades require advanced lightweight materials to maximize efficiency. Usually, nickel superalloys weighing around 8 g/cm³ are used for these applications. However, they are heavy and titanium aluminides (TiAl) based alloys offer the service at ~50% weight reduction [1]. TiAl-based alloys with a density of about 4g/cm³ are promising high-temperature materials in aero-engines, particularly those with a composition of γ/α_2 -TiAl dual phases. this TiAl-based alloy offers the advantages of low density, excellent high-temperature properties, and corrosion resistance at room temperature [1]. When in use, the TiAl components in aero-engines are exposed to high temperatures ranging from 750 to 950 °C [2], presenting challenges such as oxidation [3] and hot corrosion [4]. Despite their favourable properties, TiAl alloys are susceptible to deterioration when exposed to NaCl-Na₂SO₄ fused salts at service temperatures. These salts are formed when NaCl from marine aerosols reacts with sulphur

* Corresponding author: magogodistevens@gmail.com

dioxide from fuel gases, facilitated by the engine's heat exchange. The accumulation of these salts at high temperatures leads to hot corrosion, which is the degradation of materials due to interaction with fused salts [5]. TiAl-based alloys undergo accelerated oxidation during hot corrosion, resulting in degradation and the formation of a porous surface. The interaction between the salt agents and the material compromises the protective scale on the surface, ultimately leading to premature fractures [5, 7].

TiAl-based alloys experience poor oxidation above 800 °C. Consequently, various research studies have been conducted to enhance the oxidation resistance of these alloys within the temperature range of 700 to 900 °C. The most promising outcomes were achieved through elemental alloying such as W, Nb, Cr, and Si [8-10]. It has been discovered that the key to improving the oxidation resistance lies in the formation of a continuous layer of Al₂O₃ on the surface, rather than a mix of TiO₂/Al₂O₃ or TiO₂. The growth of TiO₂ within the Al₂O₃ layer leads to the development of micropores and cracks [6, 5]. On the surface of the TiAl alloy, TiO₂ exhibits a faster growth rate compared to the slower formation of Al₂O₃ by aluminium. Thus, it becomes challenging to achieve a pure Al₂O₃ layer on the surface without the presence of TiO₂, unless a mixture of both oxides [3]. This was consistent with an oxidation study conducted by Becker et al. [3], in which the outward-growing scale primarily comprised TiO₂, while the inward-growing scale consisted of a mixture of TiO₂ and Al₂O₃. Furthermore, TiAl alloys suffer inherent brittleness at room temperature. To address this issue, a Ti-48Al-2Nb-2Cr alloy with balanced properties for high and ambient temperature applications was developed [11]. Additionally, research by Mathabathe et al. [12, 13] identified the Ti-48Al-2Nb-0.7Cr-0.3Si alloy as having promising mechanical and thermal properties. Their study on cyclic oxidation revealed that this alloy outperformed binary Ti-48Al in terms of oxidation resistance at 900 °C, which was attributed to the precipitation of titanium silicide (Ti₅Si₃). The alloy was also reported by Ellard et al. [14] to exhibit good mechanical properties, such as improved relative density and tensile strength. The addition of Si promotes the formation of Ti₅Si₃, which enhances strength at high temperatures and forms a surface layer of silica (SiO₂). This silica layer reduces oxidation by slowing down the diffusion of oxygen into the material [15, 16].

This study aims to evaluate the hot corrosion behaviour of the arc-melted Ti-48Al-2Nb-0.7Cr-0.3Si alloy, which has shown promising properties for industrial applications. However, its performance in the presence of hot salts is crucial for its industrialization, as hot corrosion can cause accelerated oxidation. The alloy's resistance to hot corrosion will be tested under cyclic thermal loading conditions at 900 °C for 60 h, using a Na₂SO₄+(25wt.%) NaCl mixture as the salt medium. The findings from this study will contribute to a better understanding of the alloy's behaviour and potential for successful industrial application.

2 Experimental procedure

2.1 Alloy preparation

For this study, we used the fabricated TiAl intermetallic with a composition of Ti-48Al-2Nb-0.7Cr-0.3Si. It is important to note that all alloy compositions mentioned in this report are given in atomic percentage (at. %) unless otherwise specified. This TiAl-based alloy was fabricated by using pure metallic powders of Ti, Al, Nb, Cr, and Si, each with a mean particle size of 30, 74, 24, 126, and 9 µm respectively. For more detailed information on powder characterisation, please refer to reference [14]. The blended powders were compacted and melted using an electric vacuum arc furnace under an argon atmosphere, followed by furnace cooling. The casted button was then heat treated at 1250 °C for 2 h using a tube furnace in an

environment of argon gas and allowed to cool in the furnace. The button was machined into specimens measuring 12 x 12 x 2 mm³ for corrosion tests.

2.2 Hot corrosion test

The samples were ground up to 1200 SiC grit finish to allow the sticking of salts. The mass of each sample was measured before and after the corrosion tests. A mixture of 75 wt.% Na₂SO₄ + 25 wt.% NaCl salt was prepared in deionized water to form a saturated aqueous solution [17]. The saturated salt was coated on the sample surface by spraying. The samples were placed on the hot plate at about 250 °C to evaporate the moisture from the coated salt. The samples were weighed using an electronic balance to ensure a surface coating of 2 mg/cm². The sensitivity of the weighing balance used for the study was 10⁻⁴ g. The mass change was measured to establish the corrosion kinetics. The coated samples were placed in an alumina crucible and put inside a tubular high-temperature furnace. They were then heated up to 900°C for a dwell time of 60 h, with each cycle lasting 6 h. The sample was cooled in air. After each cycle, the samples were cleaned with hot water at about 80 °C using a soft brush to remove any loose particles on the surface. Then, they were dried on a hot plate and coated again with the saturated salt solution. This was done to maintain a constant concentration of corrosive agent on the surface of the samples before putting them back in the furnace. The samples were also ultrasonically cleaned for 15 minutes before each cycle.

2.3 Sample characterization

To perform characterisation and corrosion tests, samples were ground up to 1200 SiC grit, polished to a mirror-like finish and washed using deionized water and acetone for drying. For microstructural observations, the mirror-like finish samples were etched with Kroll's reagent. The microstructures were observed using optical microscopy. The surface morphologies of the hot corrosion products were observed using scanning electron microscopy (SEM) equipped with energy dispersion spectroscopy (EDS) which was used to study the elemental composition. The phases and structural development of the samples before and after the hot corrosion were performed using XRD in (2θ) angle range of 20 to 80°. The weight change per unit area (ΔW) of the samples after every hot corrosion test was calculated using Equation 1,

$$\Delta W = (m_i - m_o) / S \quad (1)$$

where ΔW is the weight change per unit area (mg/cm²), m_i is the mass of the corroded sample after a cycle (mg), m_o is the initial mass before any corrosion (mg) and S is the sample surface area in cm². After each corrosion cycle, the surface area was measured as a result of spallation.

3 Results

3.1 Alloy phase composition

The Ti-48Al-2Nb-0.7Cr-0.3Si alloy structural features such as phase composition and microstructural are presented in Fig. 1

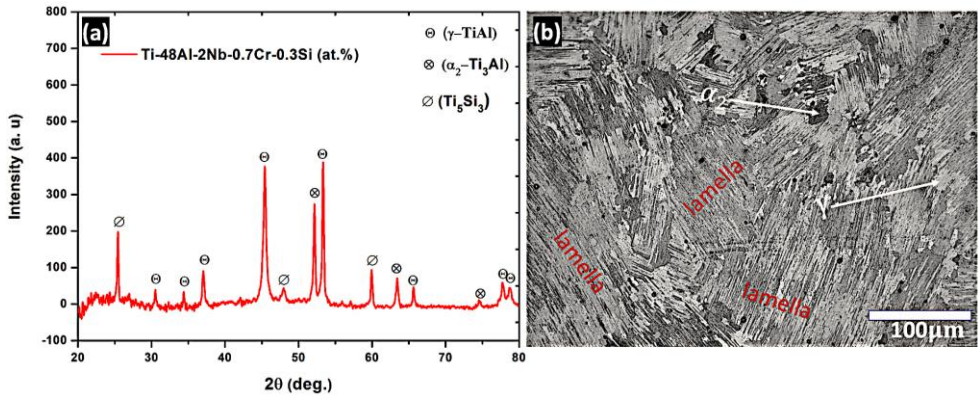


Fig. 1: (a) The XRD pattern, and (b) optical microscopy image of the Ti-48Al-2Nb-0.7Cr-0.3Si alloy.

The XRD pattern of the alloy is shown in Fig. 1 (a), and it consists of γ -TiAl, α_2 -Ti₃Al and Ti₅Si₃ phases. The microstructure of the TiAl alloy is shown by optical microscopy image in Fig. 1 (b) consisting of a nearly lamellar structure with two major phases of light grey (γ -TiAl phase with face-centred tetragonal L1₀ structure) and the dark grey (α_2 -Ti₃Al phase with close-packed hexagonal DO₁₉ structure). The alloy consists of grains (lamellar structure with the same orientation) with lamellar colonies of alternating light and dark grey phases (see Fig. 1 (b)). The grain boundaries of the alloy show an irregular serrated arrangement. The light grey regions within the lamellar colonies are γ -TiAl as they are observed to have major peaks in XRD results, while the dark grey regions are α_2 -Ti₃Al with modern peaks.

3.2 Hot corrosion performance

The cyclic hot corrosion kinetics of the Ti-48Al-2Nb-0.7Cr-0.3Si alloy was investigated at 900 °C for 60 h in air. Each cycle represents 6 h, and the kinetic curve of weight change per unit area as a function of time is represented in Fig. 2 (a).

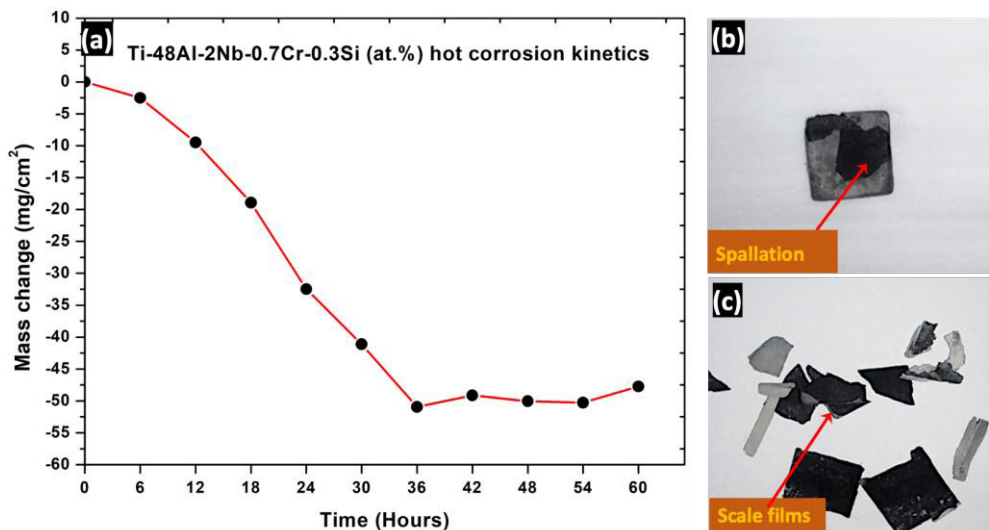


Fig. 2: (a) Hot corrosion mass change curve of the Ti-48Al-2Nb-0.7Cr-0.3Si at 900 °C for 60 h, (b) spallation, (c) scale debris.

The Ti-48Al-2Nb-0.7Cr-0.3Si alloy, suffered severe corrosion attack when it was exposed to a Na₂SO₄-25wt.%NaCl environment at 900 °C, which was higher than the melting point of the salt mixture 625 °C [18]. The alloy surface was covered by hot molten salt, which reacted with the sample and caused a mass loss of about -51 mg/cm². The oxide scale formed on the surface delaminated from the alloy after removing the sample from the furnace (see Fig. 2 b) and during the hot water cleaning. The mass change was -2.51 mg/cm² after 6 h, and then the alloy reached a stable state after 36 h due to the development of a protective scale. The dissolution of the oxide scale on the surface (see Fig. 2 (c)) contributed to the large mass change of the alloy in the salt environment. Mathabathe et al. [12, 13] conducted a study which demonstrated that the process of nitridation enhanced the cyclic oxidation resistance of the alloy. Nitridation involves the formation of a thin TiN layer on the alloy's surface, which effectively blocks the diffusion of oxygen and other corrosive agents. Consequently, the nitrided Ti-48Al-2Nb-0.7Cr-0.3Si alloy exhibited only a minor mass change of approximately -0.5 to -0.7 mg/cm² mass loss after 900 h [13]. This finding emphasizes the contrasting impact of hot corrosion attack and oxidation behaviour on the alloy. Within just 60 h, hot corrosion caused a significantly higher rate of mass loss compared to the minor mass change observed after 900 h of oxidation. These results demonstrate the greater severity of hot corrosion when compared to oxidation [13].

3.3 Scale morphology

The surface and cross-sectional microstructures of Ti-48Al-2Nb-0.7Cr-0.3Si after 60 h of cyclic hot corrosion tests are shown in Figure 3. The scale morphology on the alloy surface is depicted in Figure 3(a), while the cross-section of the scale and the alloy is illustrated in Figure 3(d).

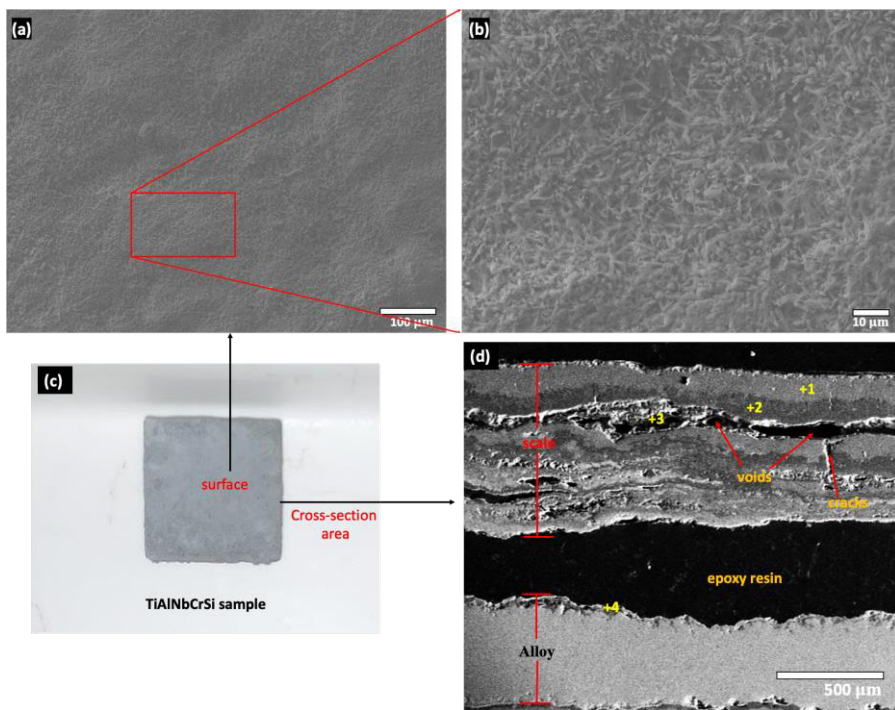


Fig 3: SEM-SEI micrographs of the Ti-48Al-2Nb-0.7Cr-0.3Si (a) low magnification, (b) high magnification of the surface, (c) 12x12mm sample photograph, (d) cross-sectional morphology.

The surface morphology of the scale appears as needle-like crystals, as shown in Fig. 3 (b). Fig. 3 (d) displays the cross-sectional microstructure, along with marked EDS spot analyses and the corresponding compositions provided in Table 1. The scales are composed of light and dark grey multilayers, as indicated by spots +1 and +2. The surface exhibiting deterioration at the scale-alloy interface can be seen in spot +4. Furthermore, in Fig. 3 (d), the oxide scale is observed to delaminate from the alloy surface, evident from the presence of epoxy division. This figure also reveals the presence of internal cracks and voids, which facilitate the migration of oxygen to the alloy-scale interface. Additionally, pitting is observed on the alloy-scale interface, resulting from the uneven surface. The overall scale has a thickness of 537 μm , while the surface TiO_2 scale measures 89 μm . Meanwhile, the bulk material itself has a thickness of 305 μm .

3.4 Phase compositions

The elemental composition of the hot corrosion products was analysed using EDS and XRD techniques. The EDS analysis, presented in Table 1 (a), provides a summary of the composition of the scale seen in Fig. 3 (a). The morphology of the scale displayed needle-like crystals that contained high levels of titanium and oxygen, while the presence of aluminium was insufficient. The high oxygen levels can be attributed to the formation of the TiO_2 rutile phase. Furthermore, there was no presence of alloying elements like Nb, Cr, and Si in the oxides. The salt medium, including Na, Cl, and S, was only observed on the surface.

Table 1: The EDS surface scale composition.

(a) Surface composition		(b) Cross-section spot analysis				
Elements	Composition (at. %)	Elements	Regional compositions (at. %)			
			+1	+2	+3	+4
Ti	23.3	Ti	36.1	1.9	-	22.3
Al	0.5	Al		40.7	-	9.8
O	59.8	O	63.9	55.7	69.0	62.9
Na	12.1	Cl	-	0.5	10.3	2.8
Cl	2.2	Si	-	0.4	-	-
S	2.1	S	-	-	14.9	-
		Cr	-	-	-	0.5

The composition analysis of the cross-sectional scale was conducted using EDS and the results are presented in Table 1 (b). Fig. 3 (d) shows a spot analysis of different areas in the scale. In spot +1, a light grey layer consisting mainly of TiO_2 is observed, while spot +2 reveals a dark grey layer composed of Al_2O_3 oxides. Spot +4 indicates a corrosion area where a mixture of TiO_2 , Al_2O_3 , TiCl_4 , Cr_2O_3 , and NbO is present, while spot +3 shows a combination of ClO_2/SO_2 oxides.

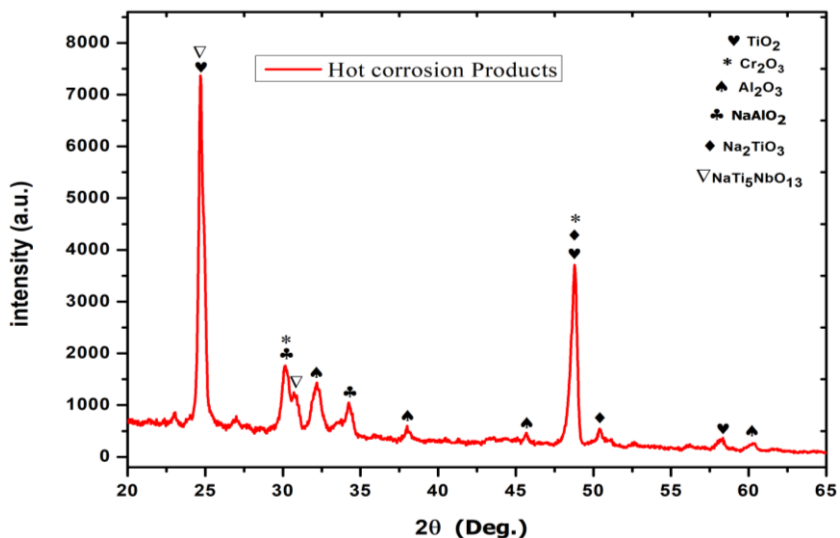


Fig 4. XRD pattern of the alloy Ti-48Al-2Nb-0.7Cr-0.3Si alloy after cyclic hot corrosion for 60 h at 900 °C.

The XRD spectra presented in Fig. 4 show the corrosion scales of Ti-48Al-2Nb-0.7Cr-0.3Si alloy after undergoing cyclic hot corrosion tests at 900°C for 60 h. These oxide scales consist of phases such as TiO₂, Al₂O₃, Na₂TiO₃, and NaTi₅NbO₁₃. Additionally, the presence of Cr₂O₃ corrosion products was observed. The visibility of α_2 and γ peaks in the spectra was affected by the presence of corrosion scales on the surface.

4 Discussion

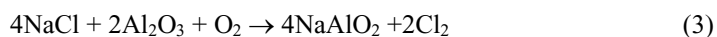
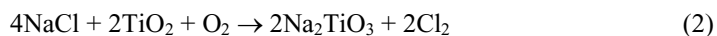
4.1 Ti-48Al-2Nb-0.7Cr-0.3Si alloy properties

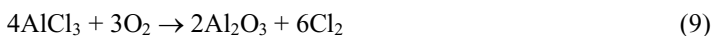
The Ti-48Al-2Nb-0.7Cr-0.3Si alloy demonstrates favourable properties compared to binary TiAl alloys [12]. According to Ellard et. al [14], the alloy exhibits good tensile properties, including a yield strength of 600MPa, an ultimate tensile stress of 850MPa, and 3% elongation. The elemental alloying of Si, Cr, and Nb has also improved the relative alloy density, enhancing the powder flowability [14, 19, 20]. In this study, the casted alloy was fabricated using vacuum arc melting [14, 20]. Microscopic analysis of the alloy revealed a lamellar structure with grains exhibiting colonies of alternating light and dark grey phases, corresponding to γ -TiAl and α_2 -Ti₃Al, respectively, as shown in Fig. 1 (b). XRD analysis confirmed the presence of γ -TiAl phase with a face-centred tetragonal L1₀ structure, represented by high-intensity peaks, hence the light grey colour (see 2 θ angles of 45, 51, and 53) [14, 20]. The dark grey regions observed in the sample were determined to be composed of the α_2 -Ti₃Al phase, which has a close-packed hexagonal DO₁₉ structure. This conclusion is supported by the low-intensity peaks observed in the XRD analysis shown in Figure 1 (a). Furthermore, a nearly lamellar microstructure was observed in the Ti-48Al-2Nb-0.7Cr-0.3Si alloy, as reported by Clemens et al. [21]. The presence of the Ti₅Si₃ phase within the alloy has also been confirmed in previous works [14] and [22]. Additionally, the Vickers microhardness of the Ti-48Al-2Nb-0.7Cr-0.3Si alloy is expected to be 289 HV, according to a study by [23].

4.2 Hot corrosion effect of Ti-48Al-2Nb-0.7Cr-0.3Si alloy.

The Ti-48Al-2Nb-0.7Cr-0.3Si alloy has demonstrated favourable oxidation properties at 900 °C, which can be attributed to surface modifications such as nitriding and alloying with Si [13]. These factors contribute significantly to the formation of a protective scale on the surface of the Ti-48Al-2Nb-0.7Cr-0.3Si alloy [12, 13]. Given the promising mechanical and oxidation properties, the Ti-Al-Nb-Cr-Si alloy was developed to investigate the impact of hot corrosion on the Ti-48Al-2Nb-0.7Cr-0.3Si alloy, as hot corrosion is an inevitable aspect during high-temperature oxidation, particularly in the presence of saltwater evaporation and sulfidation [24]. In this study, NaCl and Na₂SO₄ were used as the primary salt agents to examine the hot corrosion behaviour of the Ti-48Al-2Nb-0.7Cr-0.3Si alloy. When these salt deposits came into contact with the alloy's surface exposed to the oxidizing atmosphere, accelerated corrosion occurred. The degradation of the alloys was primarily attributed to the high reactivity of titanium and aluminium with chlorine agents. This reactivity resulted in the generation of gaseous species that penetrated the material, leading to the discontinuity of the protective scale. The presence of NaCl further accelerated the corrosion process, as the alloy underwent self-sustaining reactions. This accelerated corrosion, described in the works of [5, 6], caused mechanical stress and ultimately resulted in the formation of cracks and spallation. The investigation by Garip et al. [6] showed the high Cr-TiAl to have severe hot corrosion attack at 900 °C under Na₂SO₄ salt medium, where the loose and porous scale with the composition of Na₂Ti₃O₇, TiO₂, Al₂O₃. Mitoraj-Krolikowska et al. [5] investigated the effect of Na₂SO₄, NaCl and Na₂SO₄+NaCl mixture and reported NaCl to be more detrimental to the TiAl alloys particularly at 900 °C in air. The deterioration was attributed to the penetration of chlorine gas through the alloy's protective scale (see equations 2 to 9). Thus, contributes to various defects such as cracks, voids/pores and pits that result in scale disintegration intensified by thermal cycling. Furthermore, they reported the formation of a multilayer scale of TiO₂/Al₂O₃/TiO₂+Al₂O₃ on the surface of the alloy. In the current investigation, the Ti-48Al-2Nb-0.7Cr-0.3Si alloy exhibited severe corrosion in a Na₂SO₄+25wt.%NaCl salt environment at 900 °C, as evidenced by significant mass loss and scale spallation. The surface scale primarily comprised needle-like TiO₂ crystals, while the cross-sectional scale showed a multilayer structure consisting of TiO₂ and Al₂O₃ oxides. The analysis techniques employed also detected other corrosion products such as Na₂TiO₃, NaTi₅NbO₁₃, Cr₂O₃, TiCl₄, and ClO₂/SO₂ oxides in the scale and corrosion areas. These findings align with the literature's reports on similar corrosion mechanisms and products observed in TiAl alloys subjected to Na₂SO₄ and/or NaCl salt media [5, 6]. The intrusion of chlorine gas from the salt resulted in the formation of defects, including cracks, voids, pits, and delamination [5].

The mechanisms of degradation reactivity of TiAl with NaCl are given in equations 2 to 9. At a temperature beyond the melting point of the Na₂SO₄+NaCl mixture, sodium chloride can react with the protective scales of titanium oxide (see equation 1) and aluminium oxides (see equation 2), and then the volatile chlorine gas formed penetrates the surface of the Ti and Al (see equation 4 to 6): The chlorides of TiCl₂ and AlCl₃ can react with oxygen, and form Al₂O₃ and TiO₂ scales again (see equation 7 to 9) and the degradation process continues under the presence of NaCl salts deposits:





The cross-sectional morphology revealed that the surface scale consisted of TiO_2 on top of a mixture of $\text{Al}_2\text{O}_3/\text{TiO}_2$. XRD confirmed the presence of major peaks corresponding to these oxides. The reaction of sodium with the TiAl alloy resulted in the formation of NaAlO_2 and Na_2TiO_3 . The interaction of sodium with Nb was also evident in the $\text{NaTi}_5\text{NbO}_{13}$ phase. EDS spot analysis showed the involvement of volatile chlorides with the sample. For example, spot +3 indicated a high concentration of O_2 and Cl_2 , and spot +4 suggested the occurrence of reactions in equations 4 to 6. Moreover, spot +4 revealed the Cr_2O_3 phase. Cr_2O_3 was found to have a very detrimental effect on the material, as it accelerated the corrosion along with TiCl_4 . Chromia also caused interfacial cavities at the alloy scale, leading to scale detachment and cracking and spallation [25]. During the cooling process in an air environment, the decrease in oxygen activity significantly contributed to the plastic deformation of the scales, influencing their adhesion to the substrate, and causing detachment. This resulted in the formation of cracks and voids, further compromising the material's integrity [25]. Additionally, the cooling rate in air accelerated the disintegration of the protective scale by promoting the outward diffusion of chromium at the alloy scale interface. This phenomenon is more pronounced in air cooling, creating voids within the scale, making it easier to detach from the substrate [25]. Consequently, the material experienced increased damage and degradation due to the accelerated disintegration of the protective scale.

5 Conclusion

This study investigated the hot corrosion behaviour of the $(\alpha_2/\gamma)\text{-Ti-48Al-2Nb-0.7Cr-0.3Si}$ alloy in a $\text{Na}_2\text{SO}_4+\text{NaCl}$ environment at 900 °C for a dwell time of 60 h and the following conclusion was made:

- The corrosion kinetics of the alloy showed that the alloy experienced a severe hot corrosion attack, with a mass loss of about -50 mg/cm^2 .
- The SEM analysis revealed that the alloy formed a porous TiO_2 surface scale and a mixture of $\text{TiO}_2/\text{Al}_2\text{O}_3$, rather than a protective Al_2O_3 surface scale. The XRD analysis revealed the presence of hot corrosion products such as $\text{Na}_2\text{Ti}_3\text{O}_7$, TiO_2 , Al_2O_3 , and Cr_2O_3 .
- The presence of chlorine gas from the salt mixture was found to have a detrimental effect on the alloy, as it reacted with the scale-alloy interface and created interfacial cavities through the formation of chromia. These cavities led to scale detachment, cracking, and spallation.
- The research findings revealed that the $\text{Ti-48Al-2Nb-0.7Cr-0.3Si}$ alloy is prone to hot corrosion when exposed to a $\text{Na}_2\text{SO}_4+\text{NaCl}$ environment at elevated temperatures. As a result, it is recommended to implement surface treatment measures for the alloy to mitigate this issue.

Reference

1. T. Voisin, J. Monchoux, L. Durand, N. Karnatak, M. Thomas, A. Couret. *An innovative way to produce γ -TiAl blades: spark plasma sintering*. *Advanced Engineering Materials* 17, (10), 1408-1413, (2015).
2. T. Noda, Application of cast gamma TiAl for automobiles, *Intermetallic*, 6(7-8), pp.709-713, (1998).
3. S. Becker, A. Rahmel, M. Schorr, M. Schütze, *Mechanism of isothermal oxidation of the intermetallic TiAl and of TiAl alloys*. *Oxidation of Metals*, 38, pp.425-464, (1992).
4. Z. Tang, F. Wang, W. Wu, *Effect of a sputtered TiAlCr coating on hot corrosion resistance of gamma-TiAl*. *Intermetallic*, 7(11), pp.1271-1274, (1999).
5. M. Mitoraj-Królikowska, E. Godlewska, *Hot corrosion behaviour of (γ + α_2)-Ti-46Al-8Nb (at.%) and α -Ti-6Al-1Mn (at.%) alloys*. *Corrosion Science*, 115, pp.18-29, (2017).
6. Y. Garip, O. Ozdemir, *Comparative study of the oxidation and hot corrosion behaviours of TiAl-Cr intermetallic alloy produced by electric current activated sintering*. *Journal of Alloys and Compounds*, 780, pp.364-377, (2019).
7. Z. Tang, F. Wang, and W. Wu, *Hot-Corrosion Behaviour of TiAl-Base Intermetallic in Molten Salts*, vol. 51, pp. 235-250, (1999).
8. D.Y. Seo, T.D. Nguyen, D.B. Lee, *Oxidation of powder metallurgy (PM) Ti-48% Al-2% Cr-2% Nb-(0-1%) W alloys between 800 and 1000° C in air*. *Oxidation of metals*, 74, pp.145-156, (2010).
9. A. Brotzu, F. Felli, D. Pilone, *Effect of alloying elements on the behaviour of TiAl-based alloys*, *Intermetallics*, vol. 54, pp. 176-180, (2014).
10. K. Chou, A. Arbor, *Early oxidation behaviour of Si-coated titanium* Kathleen Chou, pp. 0-2, (1974).
11. D.M. Dimiduk, *Gamma titanium aluminide alloys—an assessment within the competition of aerospace structural materials*. *Materials Science and Engineering: A*, 263(2), pp.281-288, (1999).
12. M.N. Mathabathe, A.S. Bolokang, G. Govender, R.J. Mostert, C.W. Siyasiya, *The vacuum melted γ -TiAl (Nb, Cr, Si)-doped alloys and their cyclic oxidation properties*. *Vacuum*, 154, pp.82-89, (2018).
13. M.N. Mathabathe, A.S. Bolokang, G. Govender, C.W. Siyasiya, R.J. Mostert, *Characterization of the nitrided γ -Ti-46Al-2Nb and γ -Ti-46Al-2Nb-0.7 Cr-0.3 Si intermetallic alloys*. *Materials Chemistry and Physics*, 257, p.123703, (2021).
14. J.J.M. Ellard, M.N. Mathabathe, C.W. Siyasiya, A.S. Bolokang, *Powder characteristics blending and microstructural analysis of a hot-pack rolled vacuum arc-melted γ -TiAl-based sheet*. *South African Journal of Industrial Engineering*, 33(3), pp.274-283, (2022).
15. J. Lee, H. Park, J. Kim, J. Jang, S. Hong, *Constitutive behaviour and microstructural evolution in Ti – Al – Si ternary alloys processed by mechanical milling and spark plasma sintering*, *Integrative Medicine Research*, vol. 9, no. 2, pp. 2247-2258, (2020).
16. A. Knaislová, P. Novák, F. Průša, M. Cabibbo, L. Jaworska, D. Vojtěch, *High-temperature oxidation of Ti–Al–Si alloys prepared by powder metallurgy*, *Journal of Alloys and Compounds*, p. 151895, (2019).
17. K. Zhang, Z. Li, W. Gao, *Hot corrosion behaviour of Ti – Al based intermetallics*, vol. 57, no. December, pp. 834-843, (2002).

18. Y. Jiang, Y. Sun, R.D Jacob, F. Bruno, S. Li, *Novel Na₂SO₄-NaCl-ceramic composites as high temperature phase change materials for solar thermal power plants (Part I)*. Solar Energy Materials and Solar Cells, 178, pp.74-83, (2018).
19. J. Hlosta, D. Zurovec, L. Jezerska, J. Zegzulka, J. Necas, May. *Effect of particle shape and size on the compressibility and bulk properties of powders in powder metallurgy*. In 25th International Conference on Metallurgy and Materials, METAL (Vol. 2016, pp. 25-27), (2016).
20. N.M. Mathabathe, A.S. Bolokang, G. Govender, C.W. Siyasiya, R.J Mostert, *Cold-pressing and vacuum arc melting of γ -TiAl based alloys*. Advanced Powder Technology, 30(12), pp.2925-2939, (2019).
21. H. Clemens, S. Mayer. Design, processing, microstructure, properties, and applications of advanced intermetallic TiAl alloys. *Advanced engineering materials*, 15(4), (2013): 191-215.
22. N.M. Mathabathe, A.S. Bolokang, G. Govender, R.J. Mostert, C.W. Siyasiya, 2018. Structure-property orientation relationship of a γ/α_2 /Ti₅Si₃ in as-cast Ti-45Al-2Nb-0.7 Cr-0.3 Si intermetallic alloy. *Journal of Alloys and Compounds*, 765, pp.690-699.
23. S.M. Magogodi, M.N. Mathabathe, A.S. Bolokang, C.W. Siyasiya, *The electrochemical corrosion behaviour of Ti48Al-2Nb-0.7 Cr-0.3 Si alloy in 3.5% NaCl*, (2022).
24. N. Eliaz, G. Shemesh, R.M Latanision, *Hot corrosion in gas turbine components*. *Engineering failure analysis*, 9(1), pp.31-43 (2002).
25. P. Kofstad, High temperature corrosion. Elsevier Applied Science Publishers, Crown House, Linton Road, Barking, Essex IG 11 8 JU, UK, (1988).